mathematics

MDPI

Article

Studying the Dynamics Response of Viscoelastic Orthotropic Plates Based on Fractional-Order Derivatives and Shifted Legendre Polynomials

Qianqian Fan [1], Qiumei Liu [1,*], Yiming Chen [2], Yuhuan Cui [1,*], Jingguo Qu [1] and Lei Wang [1,3]

[1] College of Science, North China University of Science and Technology, Tangshan 063000, China; fqq@stu.ncst.edu.cn (Q.F.); qujingguo@ncst.edu.cn (J.Q.); lei.wang@ensam.eu (L.W.)
[2] School of Science, Yanshan University, Qinhuangdao 066004, China; chenym@ysu.edu.cn
[3] LISPEN, Arts et Métiers Institute of Technology, HESAM University, F-59000 Lille, France
* Correspondence: liuqiumei@ncst.edu.cn (Q.L.); cuiyh@ncst.edu.cn (Y.C.)

Abstract: This paper primarily investigates the dynamics response of viscoelastic orthotropic plates under a fractional-order derivative model, which is efficiently simulated numerically using the FKV (Fractional Kelvin–Voigt) model and the shifted Legendre polynomial algorithm. By establishing the fractional-order governing equation and directly solving it in the time domain using a shifted Legendre polynomial, the approach achieves low error and high accuracy. The analysis shows that the load, plate thickness, and creep time all affect the plate displacement, and the fractional-order model outperforms the integer-order model to better capture the dynamics response of the material.

Keywords: orthotropic plates; viscoelastic; fractional order; shifted Legendre polynomials; numerical computation; simulation of dynamics response

MSC: 35Q99

check for updates

Academic Editor: Wei-Shih Du

Received: 7 January 2025
Revised: 3 February 2025
Accepted: 9 February 2025
Published: 14 February 2025

Citation: Fan, Q.; Liu, Q.; Chen, Y.; Cui, Y.; Qu, J.; Wang, L. Studying the Dynamics Response of Viscoelastic Orthotropic Plates Based on Fractional-Order Derivatives and Shifted Legendre Polynomials. *Mathematics* **2025**, *13*, 622. https://doi.org/10.3390/math13040622

Copyright: © 2025 by the authors. Licensee MDPI, Basel, Switzerland. This article is an open access article distributed under the terms and conditions of the Creative Commons Attribution (CC BY) license (https://creativecommons.org/licenses/by/4.0/).

1. Introduction

Viscoelastic materials are esteemed for their exceptional properties across multiple fields, such as medicine, mechanics, and civil engineering [1–5]. It has been observed that traditional integer-order models, such as the Maxwell and Kelvin–Voigt models, have limitations in effectively capturing the behavior of viscoelastic materials [6]. To overcome this limitation and better simulate the complex physical behaviors of these materials, there has been a shift towards utilizing fractional-order models [7–10]. Through careful examination, it was found that fractional-order models outperform integer-order models in effectively capturing the memory characteristics of viscoelastic materials [11–13]. Fractional-order calculus and differential equations have proven to be highly beneficial in various fields of study, such as physics, biology, and mechanics [14–16]. This study seeks to enhance the prediction accuracy of the dynamic response of viscoelastic orthotropic plates through the introduction of a fractional-order derivative model, aiming to offer more dependable theoretical support for engineering applications.

To simulate the intricate response of viscoelastic materials and to efficiently solve fractional-order differential governing equations for such materials, scholars have introduced fractional-order derivatives such as Caputo, Riemann–Liouville, etc., into the traditional models to obtain new fractional-order models. Among them, Caputo fractional-order derivatives have not only been deeply developed theoretically [17,18], but also shown a

wide range of application prospects in practical applications. It is not only more suitable for describing physical phenomena but also able to maintain the initial value conditions of the original function [19], which makes the solution of equations more intuitive and convenient. In contrast, the Riemann–Liouville fractional-order derivatives require the introduction of fractional-order initial value conditions, which increases the complexity of the issue. Additionally, the researchers have extensively examined a range of numerical methods, including Galerkin [20,21], finite element techniques [22–24], and a variety of non-polynomial splines methods (covering types such as hyperbolics [25], hybrid [26], fractional [27], conformable [28], and rational splines [29]) to address these differential equations. These methods provide distinct benefits in preserving numerical stability and improving solution accuracy, offering new perspectives and approaches for the numerical resolution of fractional-order differential equations. Wang et al. [30] employed polynomial approximation techniques to address fractional-order differential equations utilizing shifted Chebyshev polynomials. Chen et al. [31] presented a numerical method for solving a class of nonlinear variable-order fractional differential equations with Legendre wavelet functions and operator matrices. Hassani et al. [32] employed Caputo-type definitions and generalized polynomials to address the Klein–Gordon equation of variable time fractional order and nonlinear. They utilized an optimization approach to obtain approximate solutions based on generalized polynomials. All these investigations confirm that the polynomial function approximation is an effective and precise method for solving fractional differential equations. In this paper, we utilize shifted Legendre polynomials for function approximation, which have shown potential for a wide range of applications in various fields such as mathematical sciences, quantum mechanics, and engineering. Zheng et al. [33] utilize a new spectral method based on the hybrid formula system of the state vector and Legendre polynomials to model guided waves in anisotropic plates. This hybrid method uses the orthogonal and recursive properties of the Legendre polynomial to simplify the integral expressions involved in all the matrices. Pagani et al. [34] present a novel one-dimensional refined model for the analysis of laminated structures. The mechanical behavior of laminated structures is effectively analyzed by integrating the Carrera Unified Formulation (CUF) with Legendre polynomial expansion. The algorithm offers substantial benefits for orthogonality, parity, and recurrence relations, which considerably streamlines the computational process and enhances numerical stability. Nonetheless, it is worth noting that the efficacy of Legendre polynomials may be constrained when dealing with highly nonlinear issues or extensive datasets, and their computational complexity may also escalate.

Recent studies have increasingly focused on orthotropic anisotropic material structures, particularly orthotropic plates, because of their unique three-way elastic symmetry plane characteristics. This has rendered them distinguished in the domain of engineering [35]. Orthotropic plates are widely employed across various industries, including aerospace, vehicle manufacturing, and electronic equipment, to fabricate structural components that must endure intricate loads and possess specific performance criteria [36–38]. Researchers have thoroughly examined many theoretical models and numerical methods to understand and simulate the complex dynamics response of orthotropic anisotropic materials [39,40]. Fractional-order calculus is essential for simulating the viscoelastic, thermal conduction, and dynamics behaviors of these materials, owing to its ability to precisely characterize their memory qualities. Hobiny et al. [41] examine the thermoelastic interactions of orthotropic anisotropic materials in a two-dimensional fractional derivative model. The researchers developed an extended thermoelastic theory, demonstrated the process of Laplace–Fourier transform inversion, and also provided numerical results. Abouelregal et al. [42] utilized a higher order time fractional derivative three-phase hysteretic heat transfer model, which

is based on fractional calculus, to analyze an infinite nonhomogeneous orthorhombic functionally gradient thermoelastic material containing spherical cavities. They then confirmed the model's validity and accuracy. Chinnaboon et al. [43] use classical plate theory and the Fractional Kelvin–Voigt (FKV) model to describe the behavioral responses of orthotropic plates on viscoelastic foundations. They also incorporate fractional-order calculus to enhance the model's accuracy in forecasting the viscoelastic response. Gao et al. [44] employed a hybrid analytical-numerical technique to solve nonlinear dynamic buckling equations, and studied the nonlinear dynamic stability of a functional gradient orthotropic anisotropic cylindrical shell placed on a two-dimensional parametric elastic foundation under linear loading and damping effects. These studies demonstrate the distinct benefits of using fractional-order models to describe the intricate physical phenomena of orthotropic material structures. It is essential to mention that while there have been previous studies on the behavioral properties and applications of orthotropic anisotropic material structures, a few studies have compared fractional-order models to integer-order models on this basis. This paper employs the shifted Legendre algorithm to approximate and solve the fractional-order governing equation for orthotropic plates. Through systematic comparison and analysis, it demonstrates that the fractional-order derivative model outperforms the traditional integer-order model in accurately describing the dynamics response of viscoelastic orthotropic plates.

This paper is organized as follows: Section 2 introduces basic knowledge, such as Caputo-type fractional-order derivatives, the FKV fractional-order model, and the shifted Legendre polynomials. Section 3 uses the FKV model to deduce and establish the partial differential fractional-order governing equation for orthotropic plates in three dimensions. In Section 4, the differential operator matrix for shifted Legendre polynomials is derived utilizing a function approximation method. In Section 5, the feasibility and accuracy of the algorithm are validated through error analysis supplemented by mathematical examples. Section 6 analyzes the displacement of orthotropic plates under time-domain harmonic loading and systematically analyzes the specific effects of plate thickness, and creep time on plate displacement, and compares a fractional-order model with an integer-order model simulating plate displacement. The conclusions are provided in Section 7.

2. Basic Knowledge

2.1. Caputo Fractional-Order Derivatives

Definition 1. *For Caputo-type fractional-order derivatives of order α, the definition can be expressed as*

$$({}_cD_t^{\alpha} f)(t) = \begin{cases} \frac{1}{\Gamma(m-\alpha)} \int_0^t \frac{f^{(m)}(\lambda)}{(t-\lambda)^{\alpha+1-m}} d\lambda, & m-1 < \alpha < m \\ \frac{d^m}{dt^m} f(t), & m = \alpha \end{cases} \tag{1}$$

where α is of fractional order and $0 < \alpha \leq 1$, ${}_cD_t^{\alpha}$ is the Caputo fractional differential operator, f is continuously differentiable at $(0, +\infty)$, m is a positive integer, and $\Gamma(z)$ is a Gamma function and $\Gamma(z) = \int_0^{\infty} e^{-t} t^{z-1} dt$.

Utilizing the aforementioned Caputo-type fractional derivative definition, we obtain

$${}_cD_t^{\alpha} t^m = \begin{cases} 0, & m = 0 \\ \frac{\Gamma(m+1)}{\Gamma(m+1-\alpha)} t^{m-\alpha}, & m = 1, 2, 3, \ldots \end{cases} \tag{2}$$

For $\alpha \in (0,1]$, $\lambda, \mu \in R$, C is a constant, $f(t) \in C^1(R)$, and the Caputo fractional differentiation has the following three properties [7,45]:

$$\begin{aligned}&(1)_c D_t^\alpha C = 0\\&(2)_c D_t^\alpha (Cf(t) = C_c D_t^\alpha f(t)\\&(3)_c D_t^\alpha [\lambda f(t) + \mu g(t)] = \lambda_c D_t^\alpha f(t) + \mu_c D_t^\alpha g(t)\end{aligned} \tag{3}$$

2.2. Fractional Kelvin–Voigt Model

This research employs the FKV model to delineate the viscoelastic characteristics of materials. Shemermergor [46] was an early pioneer in adapting the FKV model for viscoelastic materials. The FKV model is formulated by replacing the time derivative in the Kelvin–Voigt model with an α-order fractional derivative, thereby introducing a novel approach to modeling. It can be defined as

$$\sigma = (E + \eta_c D_t^\alpha)\varepsilon \tag{4}$$

In this context, σ denotes the stress, ε represents the strain, E stands for the Young's modulus of the plate, and η signifies the damping coefficient.

2.3. Shifted Legendre Polynomials

Definition 2. *The nth shift Legendre polynomial on the interval [0, 1] is denoted as follows:*

$$l_n(x) = \sum_{i=0}^{n} (-1)^{n+i} \frac{\Gamma(n+i-1)}{\Gamma(n-i+1)(\Gamma(i+1))^2} x^i \tag{5}$$

Over the interval [0, 1], the shifted Legendre polynomial can be rewritten in the form of a column vector $\varphi_n(x)$, which can be represented as a matrix product.

$$\varphi_n(x) = [l_0(x), l_1(x), ..., l_n(x)]^T = AP(x) \tag{6}$$

where $P(x) = [1, x, \ldots, x^n]^T$, $A = [a_{ij}]_{i,j=0}^{n}$, $[a_{ij}] = \begin{cases} 0, i < j \\ (-1)^{i+j} \frac{\Gamma(i+j-1)}{\Gamma(i-j+1)(\Gamma(i+1))^2}, i \geq j. \end{cases}$

When the shifted Legendre polynomial is extended from the interval [0, 1] to the interval [0, X], the shifted Legendre polynomial of degree n on interval [0, X] is denoted as follows:

$$L_n(x) = \sum_{i=0}^{n} (-1)^{n+i} \frac{\Gamma(n+i-1)}{\Gamma(n-i+1)(\Gamma(i+1))^2} \left(\frac{x}{X}\right)^i \tag{7}$$

It follows from the above that $\varphi_{n_1}(x)$ can be represented as a matrix product form when $x \in [0, X]$:

$$\varphi_{n_1}(x) = MG_1(x) \tag{8}$$

where $G_1(x) = [1, x, \ldots, x^{n_1}]^T$, $M = [m_{ij}]_{i,j=0}^{n_1}$, $[m_{ij}] = \begin{cases} 0, i < j \\ (-1)^{i+j} \frac{\Gamma(i+j-1)}{\Gamma(i-j+1)(\Gamma(i+1))^2} \left(\frac{1}{X}\right)^i, i \geq j. \end{cases}$

Similarly, when $y \in [0, Y]$, $\varphi_{n_2}(y)$ can be represented as a matrix product form

$$\varphi_{n_2}(y) = RG_2(y) \tag{9}$$

where $G_2(y) = [1, y, \ldots, y^{n_2}]^T$, $R = [r_{ij}]_{i,j=0}^{n_2}$, $[r_{ij}] = \begin{cases} 0, i < j \\ (-1)^{i+j} \frac{\Gamma(i+j-1)}{\Gamma(i-j+1)(\Gamma(i+1))^2} \left(\frac{1}{Y}\right)^i, i \geq j. \end{cases}$

Similarly, when $t \in [0, T]$, $\varphi_{n_3}(t)$ can be represented as a matrix product form

$$\varphi_{n_3}(t) = NG_3(t) \tag{10}$$

where $G_3(t) = [1, t, \ldots, t^{n_3}]^T$, $N = \left[n_{ij}\right]_{i,j=0}^{n_3}$, $\left[n_{ij}\right] = \begin{cases} 0, i < j \\ (-1)^{i+j} \frac{\Gamma(i+j-1)}{\Gamma(i-j+1)(\Gamma(i+1))^2} \left(\frac{1}{T}\right)^i, i \geq j. \end{cases}$

3. Derivation of the Governing Equation for Orthotropic Plates Utilizing the FKV Model

3.1. The Intrinsic Relationship

In this paper, we delve into the analysis of a rectangular orthotropic plate, with its length, width, and thickness denoted by a, b, and h, respectively. The surface of this plate withstands a distributed transverse load, denoted as $q(x, y, t)$.

The Caputo fractional-order derivative is employed to delineate the complex viscoelastic properties of springs. In describing the viscoelastic plate, a combination of the KV model and Caputo fractional-order derivative is utilized to form the FKV model, which contains fractional-order derivative α ($0 < \alpha \leq 1$) and can be viewed as consisting of a spring and a spring canister in parallel. The mathematical relationship between the reaction force $R = R(x, y, t)$ generated by this plate and the transverse deflection $w = w(x, y, t)$ at a point in the mid-plane of the plate is established accordingly. Subsequently, we can derive the governing equation for this orthotropic plate by applying the plate theory in classical mechanics and incorporating the reaction forces of the plate.

$$R = k_1 w + k_2 \tau^\alpha D_c^\alpha w \tag{11}$$

The intrinsic relationship of an orthotropic plate, which is the relationship between stress and strain, can be specifically expressed as follows [47]:

$$\begin{bmatrix} \sigma_{xx} \\ \sigma_{yy} \\ \sigma_{xy} \end{bmatrix} = \begin{bmatrix} Q_{11} & Q_{12} & 0 \\ Q_{12} & Q_{22} & 0 \\ 0 & 0 & Q_{33} \end{bmatrix} \begin{bmatrix} \varepsilon_{xx} \\ \varepsilon_{yy} \\ 2\varepsilon_{xy} \end{bmatrix} \tag{12}$$

where $Q_{11} = E_x/(1 - \nu_{xy}\nu_{yx})$, $Q_{12} = \nu_{xy}E_y/(1 - \nu_{xy}\nu_{yx})$, $Q_{22} = E_y/(1 - \nu_{xy}\nu_{yx})$, $Q_{66} = G_{xy}$ are elastic coefficients. In addition, the elastic modulus in the direction of x-axis and y-axis are denoted as E_x and E_y, respectively. v_{ij} (v_{xy} or v_{yx}) denotes Poisson's ratio. Poisson's ratio and elastic modulus can be related by the formula $E_x v_{yx} = E_y v_{xy}$. G_{xy} represents the shear modulus of elasticity within the x-y plane.

The displacement field at any location within the plate is represented by transverse deflection at the point in the mid-plane of this plate, which can be expressed as

$$\overline{u} = -z\frac{\partial w}{\partial x} \tag{13}$$

$$\overline{v} = -z\frac{\partial w}{\partial y} \tag{14}$$

$$\overline{w} = w \tag{15}$$

where $\overline{u}$, $\overline{v}$, and $\overline{w}$ are the displacement components along the x, y, and z at any position in the plate, respectively. Therefore, the strain of the plate can also be described in terms of transverse deflection, and the strain-displacement relationship of this plate is

$$\varepsilon_{xx} = -z\frac{\partial^2 w}{\partial x^2} \tag{16}$$

$$\varepsilon_{yy} = -z\frac{\partial^2 w}{\partial y^2} \tag{17}$$

$$\varepsilon_{xy} = -z\frac{\partial^2 w}{\partial x \partial y} \tag{18}$$

3.2. The Derivation of the Governing Equation

The governing equation for this plate can be reasoned by applying the virtual work principle as follows:

$$\delta\, U_p + \delta\, U_f + \delta V = 0 \tag{19}$$

where δU_p represents the variational definition of strain energy for the orthotropic plate, δU_f describes the variational definition of kinetic energy for the plate, and δV refers to the variational definition of external work produced by loads applied to the plate. The mathematical expression for each of these three definitions is as follows [43]:

$$\delta U_p = \int_\Omega \int_{-h/2}^{h/2} \left(\sigma_{xx}\delta\, \varepsilon_{xx} + \sigma_{yy}\delta\, \varepsilon_{yy} + 2\sigma_{xy}\delta\, \varepsilon_{xy}\right) dz d\Omega \tag{20}$$

$$\delta U_f = \int_\Omega R\, \delta w d\Omega \tag{21}$$

$$\delta V = -\int_\Omega q\, \delta w\, d\Omega \tag{22}$$

By substituting Equations (20)–(22) into Equation (19) and utilizing relation (11), then integrating over the plate's thickness, and subsequently utilizing the Gauss–Green theorem, the governing equation for the plate is derived as follows:

$$-\frac{\partial^2 M_{xx}}{\partial x^2} - 2\frac{\partial^2 M_{xy}}{\partial x \partial y} - \frac{\partial^2 M_{yy}}{\partial y^2} + k_1\, w + k_2 \tau^\alpha{}_c D^\alpha w - q = 0 \tag{23}$$

where M is the bending moment, which can be expressed as

$$M_{xx} = -\left(D_{11}\frac{\partial^2 w}{\partial x^2} + D_{12}\frac{\partial^2 w}{\partial y^2}\right) \tag{24}$$

$$M_{yy} = -\left(D_{12}\frac{\partial^2 w}{\partial x^2} + D_{22}\frac{\partial^2 w}{\partial y^2}\right) \tag{25}$$

$$M_{xy} = -2D_{66}\frac{\partial^2 w}{\partial x \partial y} \tag{26}$$

where $D_{11} = \frac{h^3}{12}Q_{11}, D_{22} = \frac{h^3}{12}Q_{22}, D_{12} = \frac{h^3}{12}Q_{12}, D_{66} = \frac{h^3}{12}Q_{66}, H = D_{12}+2D_{66}$ are plate stiffness coefficients. Q is the shear force. Q_{11}, Q_{12}, Q_{22} are mentioned in (12).

$$Q_x = -\left(D_{11}\frac{\partial^3 w}{\partial x^3} + H\frac{\partial^3 w}{\partial x \partial y^2}\right) \tag{27}$$

$$Q_y = -\left(D_{22}\frac{\partial^3 w}{\partial y^3} + H\frac{\partial^3 w}{\partial x^2 \partial y}\right) \tag{28}$$

Finally, we integrate the bending moments (24)–(26) into the governing Equation (23), and with the help of the FKV model, obtain a governing equation for a viscoelastic orthotropic plate with transverse deflection $w = w(x, y, t)$:

$$D_{11}\frac{\partial^4 w}{\partial x^4} + 2H\frac{\partial^4 w}{\partial x^2 \partial y^2} + D_{22}\frac{\partial^4 w}{\partial y^4} + k_1 w + k_2 \tau^{\alpha}{}_c D^{\alpha} w = q \tag{29}$$

Substituting $D_{11} = \frac{h^3}{12}Q_{11}, D_{22} = \frac{h^3}{12}Q_{22}, H = \frac{h^3}{12}Q_{12} + 2\frac{h^3}{12}Q_{66}, Q_{11} = E_x/(1 - \nu_{xy}\nu_{yx})$, $Q_{12} = \nu_{xy}E_y/(1 - \nu_{xy}\nu_{yx})$, $Q_{22} = E_y/(1 - \nu_{xy}\nu_{yx})$, $Q_{66} = G_{xy}$ into the governing Equation (29) gives

$$\begin{array}{l} \frac{h^3}{12}\frac{E_x}{1-v_{xy}v_{yx}}\frac{\partial^4 w}{\partial x^4} + 2\left(\frac{h^3}{12}\frac{v_{xy}E_y}{1-v_{xy}v_{yx}} + 2\frac{h^3}{12}G_{xy}\right)\frac{\partial^4 w}{\partial x^2 \partial y^2} \\ + \frac{h^3}{12}\frac{E_y}{1-v_{xy}v_{yx}}\frac{\partial^4 w}{\partial y^4} + k_1 w + k_2 \tau^{\alpha}{}_c D^{\alpha} w = q \end{array} \tag{30}$$

This plate is subject to simply supported boundary conditions, which consist of the following:

$$w = 0 \; and \; M_{xx} = 0 \; at \; x = 0 \; and \; a \tag{31}$$

$$w = 0 \; and \; M_{yy} = 0 \; at \; y = 0 \; and \; b \tag{32}$$

and assume that the initial condition $w = w(x, y, 0) = 0$.

4. Numerical Algorithms

4.1. Functional Approximation

Utilizing the vibration analysis method, the displacement function $w(x, y, t)$ in Equation (30) can be formulated as a separable variables function [48]:

$$w(x, y, t) = w(x, y)w(t) \tag{33}$$

where $w(x, y) \in L^2([0, X] \times [0, Y]), w(t) \in L^2([0, T])$.

For any continuous one-dimensional function satisfying $w(t) \in L^2([0, T])$, an approximate formula for this function can be derived using the shifted Legendre polynomial.

$$w(t) \approx \sum_{k=0}^{n_3} c_k L_k(t) = C^T \varphi_{n_3}(t) \tag{34}$$

Similarly, for any continuous two-dimensional function satisfying $w(x, y) \in L^2([0, X] \times [0, Y])$, its approximate expression is as follows:

$$w(x, y) \approx \sum_{i=0}^{n_1}\sum_{j=0}^{n_2} w_{ij} L_i(x) L_j(y) = \varphi_{n_1}^T(x) W \varphi_{n_2}(y) \tag{35}$$

The matrix form of Equation (34) can be specifically written as

$$w(t) \approx C^T \varphi_{n_3}(t) = [c_1, c_2, ..., c_{n_3}] \begin{bmatrix} L_0(t) \\ L_1(t) \\ \vdots \\ L_{n_3}(t) \end{bmatrix} \tag{36}$$

The matrix form of Equation (35) can be specifically written as

$$
\begin{aligned}
w(x,y) &\approx \varphi_{n_1}^T(x) W \varphi_{n_2}(y) \\
&= [L_0(x), L_1(x), \ldots, L_{n_1}(x)] \begin{bmatrix} w_{00} & w_{01} & \cdots & w_{0n_2} \\ w_{10} & w_{11} & \cdots & w_{1n_2} \\ \vdots & \vdots & & \vdots \\ w_{n_1 0} & w_{n_1 1} & \cdots & w_{n_1 n_2} \end{bmatrix} \begin{bmatrix} L_0(y) \\ L_1(y) \\ \vdots \\ L_{n_2}(y) \end{bmatrix}
\end{aligned} \tag{37}
$$

Therefore, the displacement function is approximated by a matrix function as

$$
w(x,y,t) \approx w(x,y) \cdot w(t) = \varphi_{n_1}^T(x) W \varphi_{n_2}(y) C^T \varphi_{n_3}(t) \tag{38}
$$

where C and W are a coefficient matrix.

4.2. Differential Operator Matrix

In the governing Equation (30), there are integer-order partial differentiators of the displacement function $\frac{\partial^4 w}{\partial x^4}$, $\frac{\partial^4 w}{\partial x^2 \partial y^2}$, $\frac{\partial^4 w}{\partial y^4}$ and fractional-order partial differentiators of the displacement function ${}_cD^{\alpha}w$. In the following, the integer-order partial differentiators and the fractional-order partial differentiators in the governing equation are replaced by using the matrix differential operator.

4.2.1. Integer-Order Differential Operators

Definition 3. *D_x^m is called a differential operator matrix of order m of shifted Legendre polynomials if there is a matrix D_x^m such that $\varphi_{n_1}^{(m)}(x) = D_x^m \varphi_{n_1}(x)$ exists.*

When m = 1, the first order differential operation of Equation (8) can be expressed as

$$
\varphi'_{n_1}(x) = (MG(x))' = MG'(x) = M \begin{bmatrix} 1' \\ x' \\ \vdots \\ (x^{n_1})' \end{bmatrix} = M \begin{bmatrix} 0 \\ 1 \\ \vdots \\ n_1 x^{n_1 - 1} \end{bmatrix} = MV_1 G(x) \tag{39}
$$

where $V_1 = [v_{ij}]_{i,j=0}^{n_1}$, $v_{ij} = \begin{cases} 0, & i \neq 1 \\ i, & i = j+1. \end{cases}$

In turn, according to Definition 3, Equation (39) can be written as

$$
\varphi'_{n_1}(x) = D_x \varphi_{n_1}(x) = D_x MG(x) \tag{40}
$$

By Equations (39) and (40), it follows that $D_x = MV_1M^{-1}$.

So, $\varphi'_{n_1}(x)$ can be rewritten as

$$
\varphi'_{n_1}(x) = D_x \varphi_{n_1}(x) = MV_1M^{-1}\varphi_{n_1}(x) \tag{41}
$$

where $D_x = MV_1M^{-1}$ is called the first order differential operator matrix of the shifted Legendre polynomials.

When m = 2, the second-order differential operation of Equation (8) can be expressed as

$$
\varphi''_{n_1}(x) = \left(\varphi'_{n_1}(x)\right)' = MV_1M^{-1}\varphi'_{n_1}(x) = \left(MV_1M^{-1}\right)^2 \varphi_{n_1}(x) = D_x^2 \varphi_{n_1}(x) \tag{42}
$$

where $D_x^2 = \left(MV_1M^{-1}\right)^2$ is called the second-order differential operator matrix of the shifted Legendre polynomials.

Similarly, one can derive the m-order differential operator matrix of the shifted Legendre polynomials as

$$\varphi_{n_1}^{(m)}(x) = {}_cD_x^m \varphi_{n_1}(x) = \left(Mv_1M^{-1}\right)^m \varphi_{n_1}(x) \tag{43}$$

$$\varphi_{n_2}^{(m)}(y) = {}_cD_y^m \varphi_{n_2}(y) = \left(Rv_2R^{-1}\right)^m \varphi_{n_2}(y) \tag{44}$$

$$\varphi_{n_3}^{(m)}(t) = {}_cD_t^m \varphi_{n_3}(t) = \left(Nv_3N^{-1}\right)^m \varphi_{n_3}(t) \tag{45}$$

By substituting Equations (46)–(48) into Equation (38), the integer-order partial differentiators of the displacement function involved in the governing Equation (30) can be derived as follows:

$$\begin{aligned} \frac{\partial^4 w(x,y,t)}{\partial x^4} &\approx \frac{\partial^4\left(\varphi_{n_1}^T(x)W\varphi_{n_2}(y)C^T\varphi_{n_3}(t)\right)}{\partial x^4} = \frac{\partial^4\varphi_{n_1}^T(x)}{\partial x^4}W\varphi_{n_2}(y)C^T\varphi_{n_3}(t) \\ &= \varphi_{n_1}^T(x)\left(\left(Mv_1M^{-1}\right)^T\right)^4 W\varphi_{n_2}(y)C^T\varphi_{n_3}(t) \end{aligned} \tag{46}$$

$$\begin{aligned} \frac{\partial^4 w(x,y,t)}{\partial x^2y^2} &\approx \frac{\partial^4\left(\varphi_{n_1}^T(x)W\varphi_{n_2}(y)C^T\varphi_{n_3}(t)\right)}{\partial x^2y^2} = \frac{\partial^2\varphi_{n_1}^T(x)}{\partial x^2}W\frac{\partial^2\varphi_{n_2}(y)}{\partial y^2}C^T\varphi_{n_3}(t) \\ &= \varphi_{n_1}^T(x)\left(\left(Mv_1M^{-1}\right)^T\right)^2 W\left(Rv_2R^{-1}\right)^2\varphi_{n_2}(y)C^T\varphi_{n_3}(t) \end{aligned} \tag{47}$$

$$\begin{aligned} \frac{\partial^4 w(x,y,t)}{\partial y^4} &\approx \frac{\partial^4\left(\varphi_{n_1}^T(x)W\varphi_{n_2}(y)C^T\varphi_{n_3}(t)\right)}{\partial y^4} = \varphi_{n_1}^T(x)W\frac{\partial^4\varphi_{n_2}(y)}{\partial y^4}C^T\varphi_{n_3}(t) \\ &= \varphi_{n_1}^T(x)W\left(Rv_2R^{-1}\right)^4\varphi_{n_2}(y)C^T\varphi_{n_3}(t) \end{aligned} \tag{48}$$

4.2.2. Fractional-Order Differential Operators

Definition 4. *K_t denotes the fractional-order operator matrix of the shifted Legendre polynomial if there is a matrix K_t such that $D_t^\alpha\varphi_{n_3}(t) = K_t\varphi_{n_3}(t)$ exists.*

According to the definition of the Caputo derivative, the fractional-order derivative of the α-order of t^{n_3} can be denoted as ${}_cD_t^\alpha t^{n_3} = \frac{\Gamma(n_3+1)}{\Gamma(n_3+1-\alpha)}t^{n_3-\alpha}$.

And according to (10), there is again a fractional-order operator matrix K_t satisfying ${}_cD_t^\alpha\varphi_{n_3}(t) = K_t\varphi_{n_3}(t)$. So it can be obtained as follows:

$$\begin{aligned} {}_cD_t^\alpha\varphi_{n_3}(t) = {}_cD_t^\alpha(NG(t)) = N_cD_t^\alpha G(t) &= N_cD_t^\alpha\begin{bmatrix} 1 \\ t \\ \vdots \\ t^{n_3} \end{bmatrix} \\ = N\begin{bmatrix} 0 \\ \frac{\Gamma(2)}{\Gamma(2-\alpha)}t^{1-\alpha} \\ \vdots \\ \frac{\Gamma(n_3+1)}{\Gamma(n_3+1-\alpha)}t^{n_3-\alpha} \end{bmatrix} &= NQG(t) \end{aligned} \tag{49}$$

And (10) can be rewritten as $G(t) = N^{-1}\varphi_{n_3}(t)$, so the above equation can also be written as

$${}_cD_t^\alpha\varphi_{n_3}(t) = NQN^{-1}\varphi_{n_3}(t) \;=\; K_t\varphi_{n_3}(t) \tag{50}$$

Referring to Section 4.1, this formula is carried over to the fractional-order operators of the governing equation to obtain

$$\begin{aligned} {}_cD^{\alpha}w(x,y,t) &\approx {}_cD^{\alpha}\left(\varphi_{n_1}^T(x)W\varphi_{n_2}(y)C^T\varphi_{n_3}(t)\right) \\ &= \varphi_{n_1}^T(x)W\varphi_{n_2}(y)C^T{}_cD^{\alpha}(\varphi_{n_3}(t)) \\ &= \varphi_{n_1}^T(x)W\varphi_{n_2}(y)C^TNQN^{-1}\varphi_{n_3}(t) \end{aligned} \tag{51}$$

4.3. Operator Matrix Form of the Governing Equation

The differential operators of integer and fractional-order obtained above are brought into Equation (30), and the governing equation containing the differential operator matrix obtained after collation is as follows:

$$\begin{aligned} &\tfrac{h^3}{12}\tfrac{E_x}{1-v_{xy}v_{yx}}\varphi_{n_1}^T(x)\left(\left(Mv_1M^{-1}\right)^T\right)^4W\varphi_{n_2}(y)C^T\varphi_{n_3}(t) \\ &+2\left(\tfrac{h^3}{12}\tfrac{v_{xy}E_y}{1-v_{xy}v_{yx}}+2\tfrac{h^3}{12}G_{xy}\right)\varphi_{n_1}^T(x)\left(\left(Mv_1M^{-1}\right)^T\right)^2W\left(Rv_2R^{-1}\right)^2\varphi_{n_2}(y)C^T\varphi_{n_3}(t) \\ &+\tfrac{h^3}{12}\tfrac{E_y}{1-v_{xy}v_{yx}}\varphi_{n_1}^T(x)W\left(Rv_2R^{-1}\right)^4\varphi_{n_2}(y)C^T\varphi_{n_3}(t)+k_1w \\ &+k_2\tau^{\alpha}\varphi_{n_1}^T(x)W\varphi_{n_2}(y)C^TNQN^{-1}\varphi_{n_3}(t)=q \end{aligned} \tag{52}$$

The boundary conditions containing the differential operator matrix are as follows:

$$w(0,y,t) \approx \varphi_{n_1}^T(0)W\varphi_{n_2}(y)C^T\varphi_{n_3}(t) = 0 \tag{53}$$

$$w(a,y,t) \approx \varphi_{n_1}^T(a)W\varphi_{n_2}(y)C^T\varphi_{n_3}(t) = 0 \tag{54}$$

$$w(x,0,t) \approx \varphi_{n_1}^T(x)W\varphi_{n_2}(0)C^T\varphi_{n_3}(t) = 0 \tag{55}$$

$$w(x,a,t) \approx \varphi_{n_1}^T(x)W\varphi_{n_2}(a)C^T\varphi_{n_3}(t) = 0 \tag{56}$$

$$\begin{aligned} M_{xx}(0,y,t) \approx &-\tfrac{h^3}{12}\tfrac{E_x}{1-v_{xy}v_{yx}}\varphi_{n_1}^T(0)\left(\left(Mv_1M^{-1}\right)^T\right)^2W\varphi_{n_2}(y)C^T\varphi_{n_3}(t) \\ &-\tfrac{h^3}{12}\tfrac{v_{xy}E_y}{1-v_{xy}v_{yx}}\varphi_{n_1}^T(0)W\left(Rv_2R^{-1}\right)^2\varphi_{n_2}(y)C^T\varphi_{n_3}(t)=0 \end{aligned} \tag{57}$$

$$\begin{aligned} M_{xx}(a,y,t) \approx &-\tfrac{h^3}{12}\tfrac{E_x}{1-v_{xy}v_{yx}}\varphi_{n_1}^T(a)\left(\left(Mv_1M^{-1}\right)^T\right)^2W\varphi_{n_2}(y)C^T\varphi_{n_3}(t) \\ &-\tfrac{h^3}{12}\tfrac{v_{xy}E_y}{1-v_{xy}v_{yx}}\varphi_{n_1}^T(a)W\left(Rv_2R^{-1}\right)^2\varphi_{n_2}(y)C^T\varphi_{n_3}(t)=0 \end{aligned} \tag{58}$$

$$\begin{aligned} M_{yy}(x,0,t) \approx &-\tfrac{h^3}{12}\tfrac{v_{xy}E_y}{1-v_{xy}v_{yx}}\varphi_{n_1}^T(x)\left(\left(Mv_1M^{-1}\right)^T\right)^2W\varphi_{n_2}(0)C^T\varphi_{n_3}(t) \\ &-\tfrac{h^3}{12}\tfrac{E_y}{1-v_{xy}v_{yx}}\varphi_{n_1}^T(x)W\left(Rv_2R^{-1}\right)^2\varphi_{n_2}(0)C^T\varphi_{n_3}(t)=0 \end{aligned} \tag{59}$$

$$\begin{aligned} M_{yy}(x,a,t) \approx &-\tfrac{h^3}{12}\tfrac{v_{xy}E_y}{1-v_{xy}v_{yx}}\varphi_{n_1}^T(x)\left(\left(Mv_1M^{-1}\right)^T\right)^2W\varphi_{n_2}(a)C^T\varphi_{n_3}(t) \\ &-\tfrac{h^3}{12}\tfrac{E_y}{1-v_{xy}v_{yx}}\varphi_{n_1}^T(x)W\left(Rv_2R^{-1}\right)^2\varphi_{n_2}(a)C^T\varphi_{n_3}(t)=0 \end{aligned} \tag{60}$$

By employing the collocation method, the variable (x,y,t) is discretized into (x_i,y_j,t_k) by taking nodes. Equation (52) and boundary conditions are converted to algebraic equations. The unknown coefficient matrices are computed using the least squares method and Matlab software (version 9.9). Substituting the coefficient matrices into Equation (52) yields a numerical solution to the fractional-order differential equation in the time domain.

5. Error Analysis and Numerical Examples

5.1. Error Analysis

The following theorem will demonstrate the feasibility of approximating the ternary displacement function using the shifted Legendre polynomial. The ternary function $u(x,y,t)$ can be decomposed by Equation (33) into $u(x,y)u(t)$. Thus, an approximation theorem for $u(x,y)$ is given. The same approach applies to the approximation of the function $u(t)$.

Theorem 1. *Suppose $u(x,y)$ is a smooth function on [0, 1] × [0, 1] and $u_n(x,y)$ is the best approximation of $u(x,y)$. These two functions follow the following relation:*

$$||u(x,y) - u_n(x,y)||_2 \leq C_1(\frac{1}{M})^{M+1} + C_2(\frac{1}{N})^{N+1} + C_3(\frac{1}{M})^{M+1}(\frac{1}{N})^{N+1} \tag{61}$$

where

$$C_1 = \frac{1}{4} \max_{(x,y)\in[0,1]\times[0,1]} \left| \frac{\partial^{M+1}}{\partial x^{M+1}} u(x,y) \right| \tag{62}$$

$$C_2 = \frac{1}{4} \max_{(x,y)\in[0,1]\times[0,1]} \left| \frac{\partial^{N+1}}{\partial y^{N+1}} u(x,y) \right| \tag{63}$$

$$C_3 = \frac{1}{16} \max_{(x,y)\in[0,1]\times[0,1]} \left| \frac{\partial^{M+N+2}}{\partial x^{M+1}\partial y^{N+1}} u(x,y) \right| \tag{64}$$

From the above theorem, it can be shown that $u_n(x,y)$ converges consistently $u(x,y)$. Similarly, it can be shown that $u_n(t)$ converges consistently to $u(t)$. The detailed proof process can be referred to in the literature [49,50]. In summary, it can be shown that the shifted Legendre polynomial is feasible to approximate ternary unknown functions.

5.2. Numerical Examples

In this section, we verify the validity and accuracy of the algorithm for solving fractional-order equations by comparing the analytical solution with the numerical solution through a mathematical arithmetic example. As a numerical example, the following equation, which is similar to (29), is used as a numerical example. The parameters in the examples are set arbitrarily and they do not represent actual physical quantities or specific meanings. The specific equation is given as follows:

$$10\frac{\partial^4 w}{\partial x^4} + \frac{\partial^4 w}{\partial x^2 \partial y^2} + 5\frac{\partial^4 w}{\partial y^4} + 90000w + 100000\tau^\alpha {}_c D^\alpha w = q \tag{65}$$

where the boundary conditions are defined as follows:

$$w(x,y,t)|_{x=0,1} = 0 \tag{66}$$

$$w(x,y,t)\big|_{y=0,1} = 0 \tag{67}$$

$$M_{xx}(x,y,t)|_{x=0,1} = 0 \tag{68}$$

$$M_{yy}(x,y,t)\big|_{y=0,1} = 0 \tag{69}$$

The equation has the following exact solution:

$$\omega(x,y,t) = \sin\left(\frac{\pi x}{a}\right)\cos\left(\frac{\pi y}{b}\right)t^2 \tag{70}$$

when $\alpha = 0.4, \tau = 1, x, y, t \in [0,1]$, substituting the exact solution into (65) yields q by deduction:

$$\begin{aligned} q = &\left(D_{11}\tfrac{\pi^4}{a^4} + 2H\tfrac{\pi^4}{a^4} + D_{22}\tfrac{\pi^4}{a^4} + k_1\right)\sin\left(\tfrac{\pi x}{a}\right)\sin\left(\tfrac{\pi y}{b}\right)t^2 \\ &+k_2 t^\alpha \sin\left(\tfrac{\pi x}{a}\right)\sin\left(\tfrac{\pi y}{b}\right)\tfrac{\Gamma(3)}{\Gamma(3-\alpha)}t^{2-\alpha} \end{aligned} \tag{71}$$

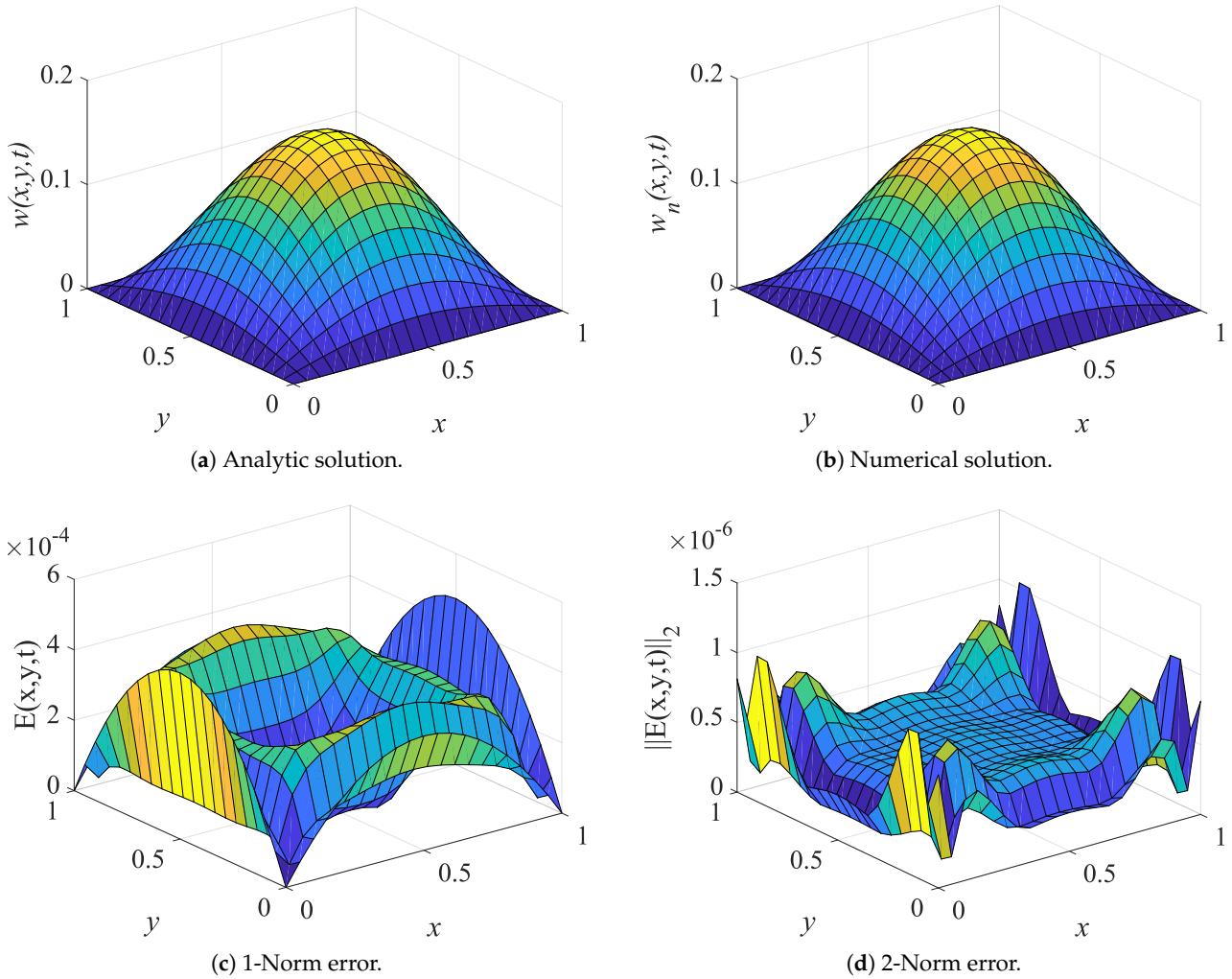
It is solved by the shifted Legendre polynomial algorithm with $n = 4$. The numerical solution is $w_n(x, y, t)$, and the 1-Norm error (i.e., absolute error) is

$$E(x, y, t) = |w_n(x, y, t) - w(x, y, t)| \tag{72}$$

In addition to this, when we are solving mathematical problems, especially where polynomial approximation or interpolation is involved, the use of the 2-Norm as a measure of the cumulative effect of the error is a common and effective method. The 2-Norm error corresponding to the above math example is

$$\|E(x, y, t)\|_2 = \sqrt{\sum_{i=1}^{n} E(x_i, y_i, t_i)^2} \tag{73}$$

Figure 1a and Figure 1b below represent the analytical and numerical solutions at $t = 0.4$ s, respectively. It can be observed that the numerical solution aligns well with the analytical solution. Figure 1c shows the 1-Norm error, whose maximum order of magnitude can still be up to 10^{-4}. Figure 1d shows the 2-Norm error, whose maximum order of magnitude can still be up to 10^{-6}. The results indicate that the algorithm is feasible in solving the fractional-order governing equation of orthotropic plates with high accuracy.



(**a**) Analytic solution.

(**b**) Numerical solution.

(**c**) 1-Norm error.

(**d**) 2-Norm error.

Figure 1. Solutions and errors.

All numerical calculations were executed using MATLAB R2017b on a Laptop equipped with an Intel Core i9-12900H processor running at 2.26 GHz and 16 GB of RAM.

6. Dynamics Analysis

This section assumes that the orthotropic plates are fabricated from graphite-epoxy resin, whose material properties are listed in Table 1. The effect of the parameters in the governing equation of viscoelastic orthotropic plates on the bending behavior of orthotropic plates is analyzed by studying the parameters in the governing equation, which involve the external loads and the nature of the plates.

Table 1. Material properties of graphite-epoxy resin.

Performance	Values	Units
x-axis modulus of elasticity E_x	140.68	GPa
y-axis modulus of elasticity E_y	9.13	GPa
Shear modulus of elasticity G_{xy}	7.24	GPa
Poisson's ratio v_{xy}	0.3	

6.1. Effect of Different Harmonic Loads on Plate Displacement

This section provides a detailed analysis of the impact of various harmonic loads on plate displacements. Holding the loading time, fractional order, and creep time constant, we analyze harmonic loads of the form $F = a\sin(\omega t) + b$ and pay special attention to how the amplitude a and frequency ω affect the plate displacement. Since an increase in b is tantamount to applying a uniform additional load across the plate, which in turn leads to an increase in plate displacement, we do not discuss the impact of b individually in this study section. Below we simulate the variation in the displacement along the y-axis at x = 0.1, 0.2, 0.3, 0.4, and 0.5 for different harmonic load conditions.

6.1.1. Variation of the Amplitude a

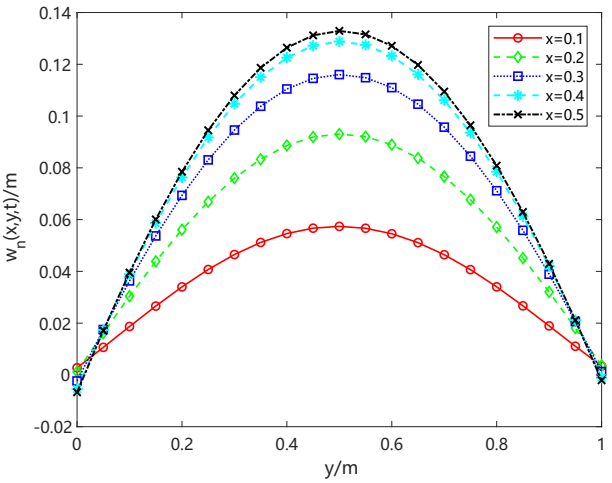
Figure 2a illustrates that when the harmonic load is $F = 15\pi\sin(2t)$, the displacement of the plate at designated point x = 0.5, y = 0.5 achieves a value of 0.1329. When the amplitude a in Figure 2b is increased to 20π (i.e., $F = 20\pi\sin(2t)$), the displacement at the same position increases to 0.1399. Moreover, in Figure 2c, it is evident that when the amplitude a is 25π (i.e., $F = 25\pi\sin(2t)$), the displacement attains a value of 0.1467. The results unambiguously demonstrate that when the amplitude a grows, the displacement at the point also increases.

This is in complete conformity with the principles of physics, as the amplitude a establishes the maximum value of the Harmonic load, which is the intensity of the force. When the material qualities and boundary conditions are kept constant, the greater the strength of the force, the greater the displacement response of the plate.

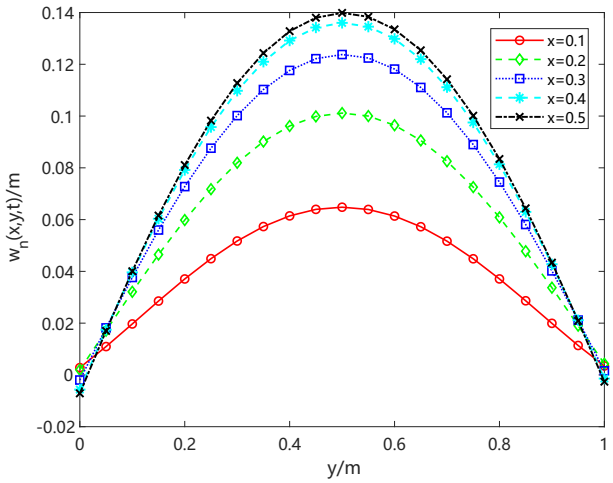
6.1.2. Variation of the Frequency ω

In Figure 3a, it is shown that when the harmonic load is given by $F = 20\pi\sin(1.5t)$ (i.e., $\omega = 1.5$), the displacement of the plate at specified point x = 0.5, y = 0.5 is measured to be 0.1347. When the frequency ω is increased to 2 (i.e., $F = 20\pi\sin(2t)$ as depicted in Figure 3b), the displacement of the same position rose to 0.1399. In addition, when the frequency rate ω was further raised to 2.2 (i.e., $F = 20\pi\sin(2.2t)$, as depicted in Figure 3c), the displacement experienced a minor increase to 0.1407. Based on these data, it is evident that as the frequency ω increases, the displacement of the plate at specified point x = 0.5, y = 0.5 likewise increases.

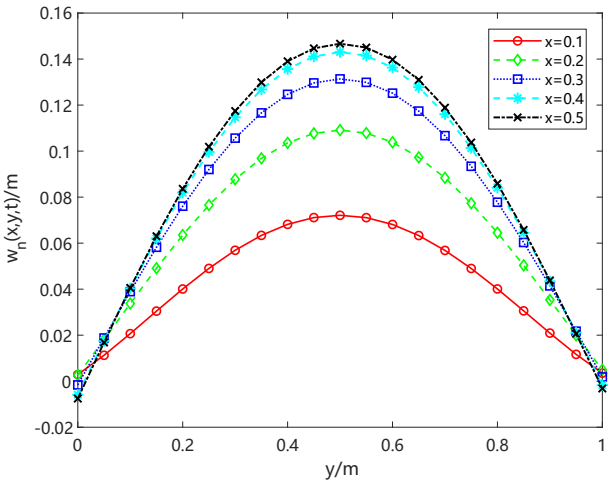
This is in accordance with the laws of physics, as an increase in frequency means more changes in force per unit of time, which may lead to a greater cumulative effect and hence an increase in displacement.



(**a**) $F = 15\pi \sin(2t)$.



(**b**) $F = 20\pi \sin(2t)$.



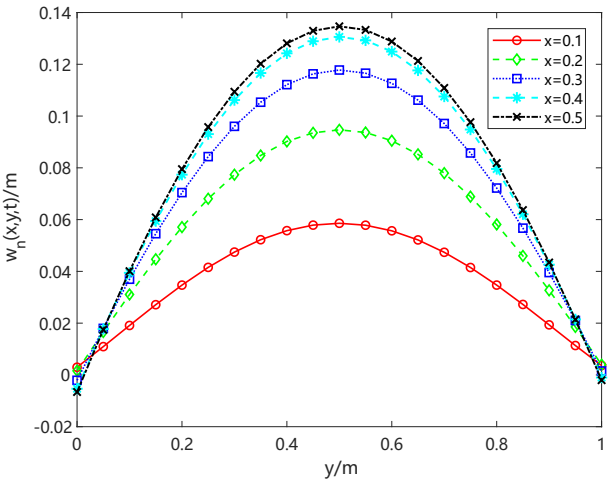
(**c**) $F = 25\pi \sin(2t)$.

Figure 2. The effect of the amplitude a on plate displacement.

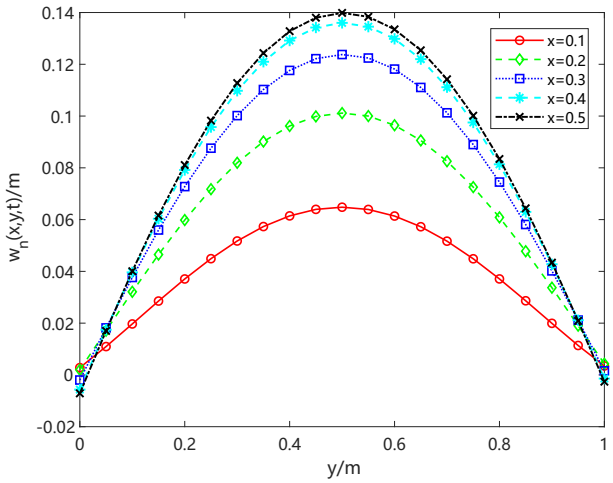
6.2. Effect of Plate Thickness on Plate Displacement

We conducted a simulation to determine the displacement of plates with varying thicknesses (h = 0.03, 0.04, 0.06) while keeping the force, fractional order, loading time, and creep time. The simulation results demonstrate that the displacement graphs of plates with varying thicknesses align precisely with the actual displacements. Additionally, the displacements at the highest point gradually decrease as the plate thickness increases, as depicted in Figure 4a–c.

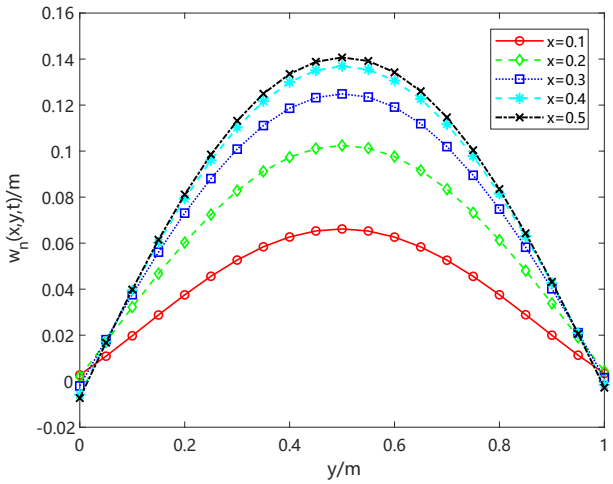
This phenomenon can be elucidated by considering both the plate's structure and the mechanical properties of the material. Structurally, under the same stress conditions, thicker plates possess a greater cross-sectional area, enabling them to withstand external stresses better and reduce displacement. Additionally, from the point of view of the mechanical properties of the material, thicker plates possess greater stiffness and can better keep their shape stable. Consequently, a plate with greater thickness will demonstrate reduced displacement when subjected to identical force conditions and creep time. This information provides a valuable reference for engineering design and material selection. For practical purposes, we can select the suitable plate thickness based on the desired displacement range and structural criteria.



(**a**) $F = 20\pi \sin(1.5t)$.



(**b**) $F = 20\pi \sin(2t)$.



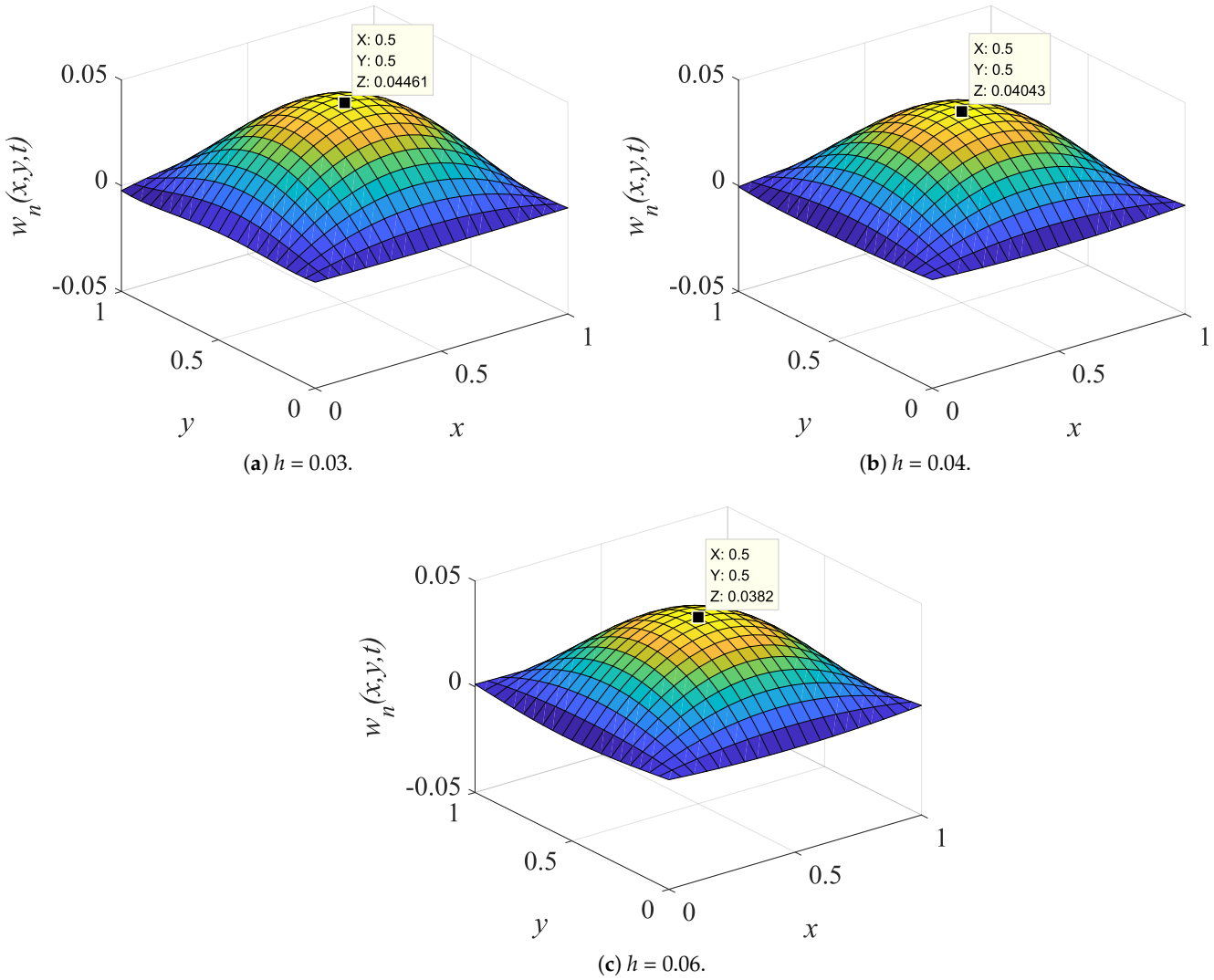
(**c**) $F = 20\pi \sin(2.2t)$.

Figure 3. The effect of the frequency ω on plate displacement.

6.3. Effect of Fractional Order on Plate Displacement

In this section, we explore the simulation effect of the model for plate displacement under constant external force and creep time conditions with different fractional-order derivatives. Specifically, we systematically analyze the characteristics of the displacement response curves predicted by the model at different fractional-order α and integer order.

The results of this study show that, as shown in Figure 5a–c, when modeled with fractional-order derivatives (e.g., α equals 0.4, 0.65, and 1.2), the model is able to more accurately fit the displacement response of the plate, and the obtained results are highly consistent with the displacement change curves of the plate after stressing in the actual case. In contrast, as shown in Figure 5d, when simulations are performed using integer-order derivatives (e.g., α equals 1), the predictions of the model deviate somewhat from the actual displacement response curves. This finding suggests that the fractional-order derivative model has significant advantages in capturing the complex, nonlinear behavior of the material during the stressing process, and is able to reflect the actual mechanical response of the material more realistically.



(**a**) $h = 0.03$. (**b**) $h = 0.04$.

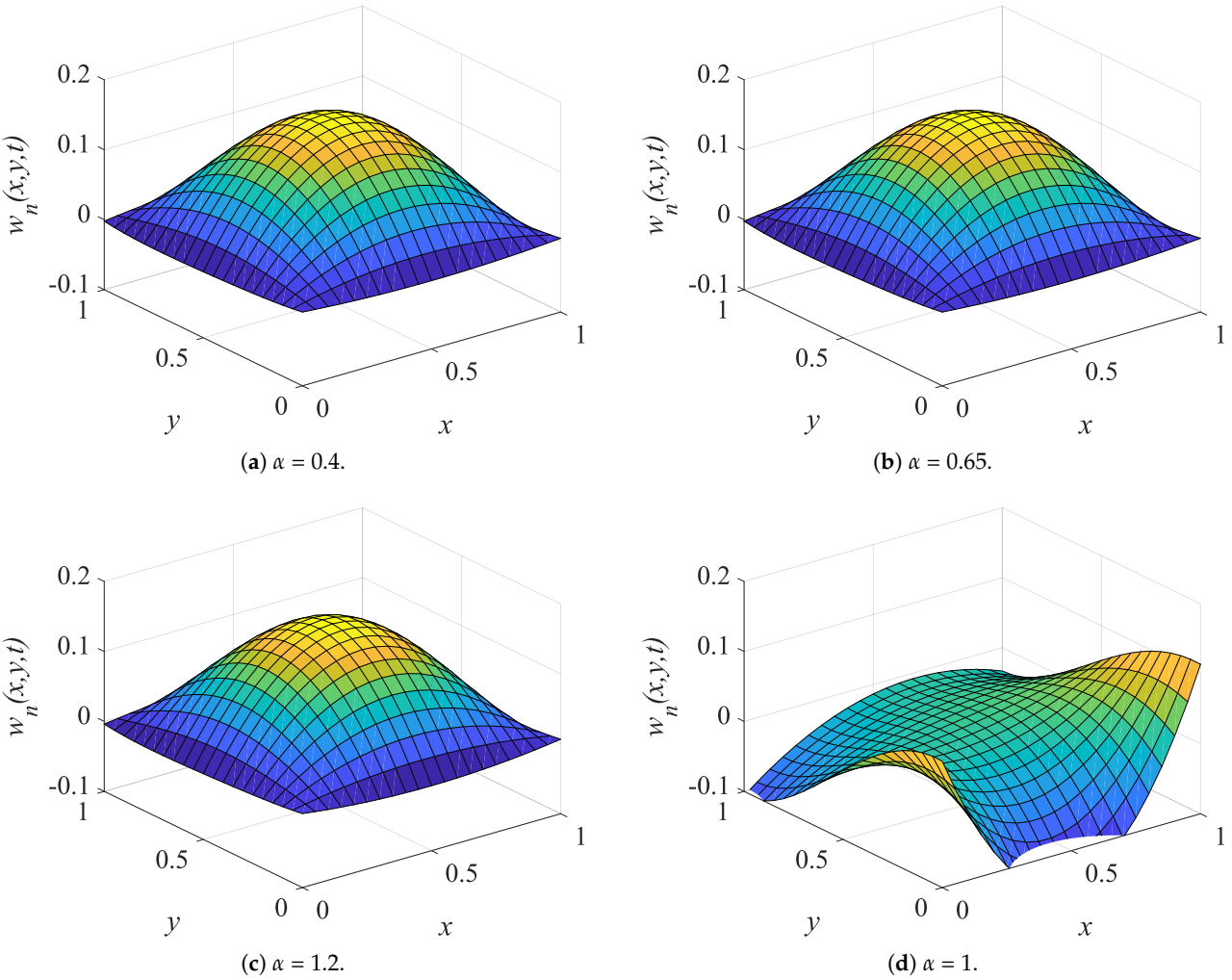
(**c**) $h = 0.06$.

Figure 4. Displacement of plates of different thicknesses.

Further, as shown in Figure 6, it appears overall that the maximum value of plate displacement is increasing with time when α takes different values.And when α takes different values, respectively, the variation in the maximum value of the plate displacement is separated by a characteristic point, and the relationship between the value of α taken and the maximum value of the plate displacement is different for the left and right sides of the characteristic point. This law is consistent with the conclusion of the literature [43], and the characteristic point changes with creep time.

6.4. Effect of Creep Time on Plate Displacement

In this section, we investigate the effect of different creep times τ on the displacement of a specific point ($x = 0.5$, $y = 0.5$) on a plate at a specific fractional order (i.e., α equals 0.2 and 0.4) and at a constant loading time, as shown in Tables 2 and 3. Creep is a phenomenon of the continuous deformation of materials under constant stress with time, and its properties are of great importance in the field of materials science and engineering. Time t and creep time τ are two different time variables.



(**a**) $\alpha = 0.4$. (**b**) $\alpha = 0.65$.

(**c**) $\alpha = 1.2$. (**d**) $\alpha = 1$.

Figure 5. Simulation of plate displacement at different fractional orders.

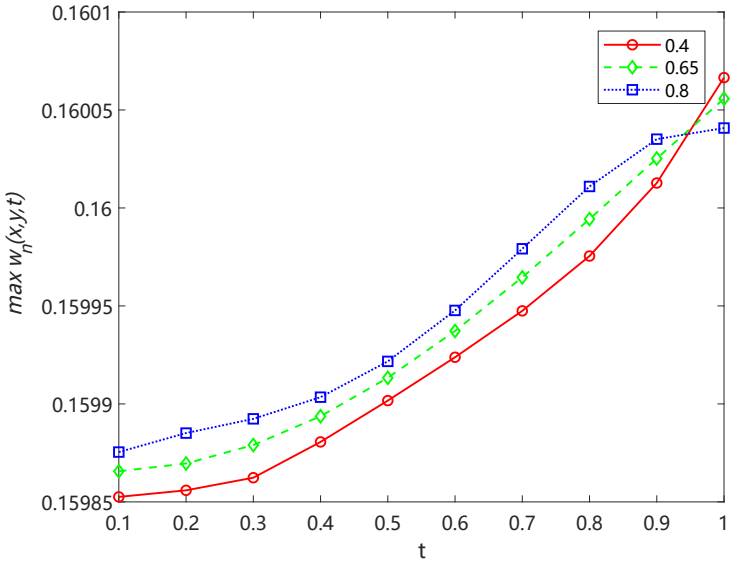
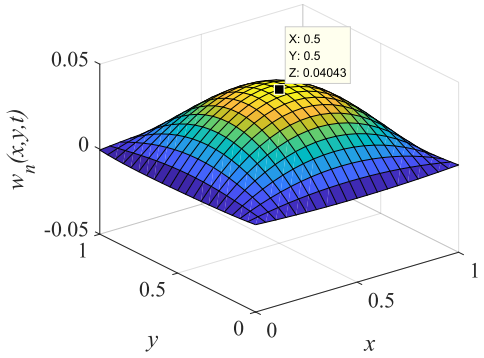
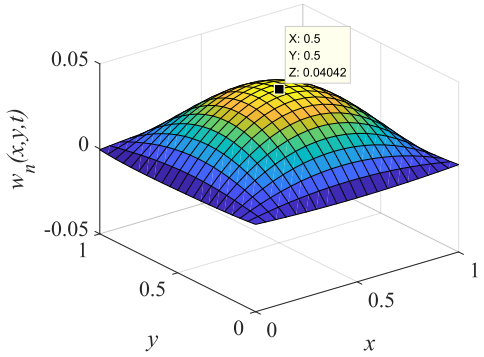
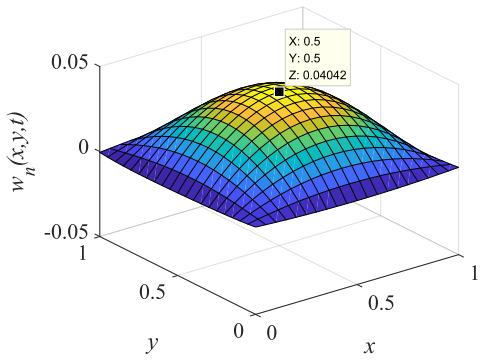


Figure 6. Variation of $maxw_n$ with time t for different α at $\tau = 1$.

First, we take the case of α equals 0.2 as an example to analyze, as shown in Table 2. By observing and comparing the displacement images under different creep times, we can find that all the displacement images are consistent with the physical laws of actual

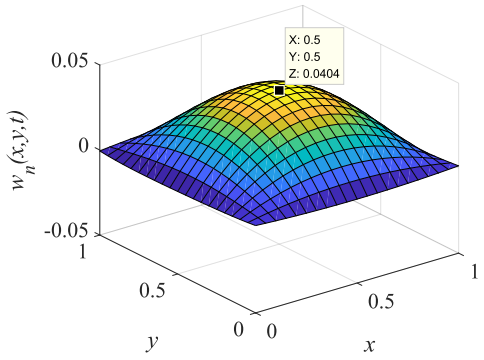
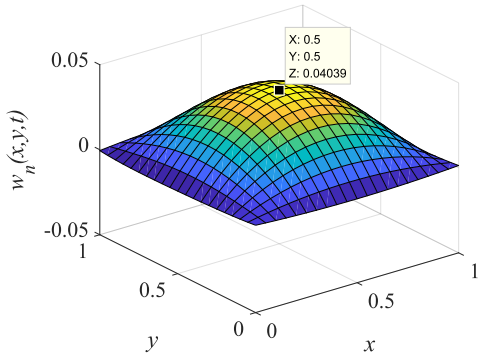
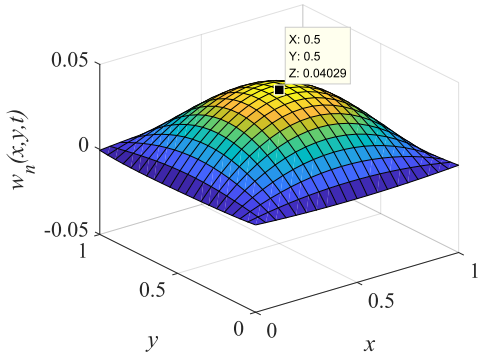
displacement changes. Specifically, when the creep time τ is 10, the displacement value of the point is 0.0404263248311901; as the creep time τ increases to 20, the displacement value slightly decreases to 0.0404240248710870, and when the creep time τ further increases to 60, the displacement value continues to decrease to 0.0404187776128624.

Table 2. Effect of creep time variation on plate displacement when $\alpha = 0.2$.

$\alpha = 0.2$	$w_n(x, y, t)$	Picture
$\tau = 10$	0.0404263248311901	
$\tau = 20$	0.0404240248710870	
$\tau = 60$	0.0404187776128624	

Next, we analyze the case when α equals 0.4, as shown in Table 3. Similarly, we find that the effect of creep time on displacement shows the same trend. Based on the above data, it can be concluded that comparing different creep times at a certain fractional order, the larger the creep time, the smaller the deflection at the highest point of the plate. And under a certain creep time, comparing different fractional orders, the larger the fractional order, the smaller the deflection at the highest point of the plate. These conclusions are in agreement with those in the literature [43] regarding creep time and plate displacement.

Table 3. Effect of creep time variation on plate displacement when $\alpha = 0.4$.

$\alpha = 0.4$	$w_n(x, y, t)$	Picture
$\tau = 10$	0.0404043828926406	
$\tau = 20$	0.0403947593429376	
$\tau = 60$	0.0402924154856163	

7. Conclusions

In this paper, the dynamics response of a viscoelastic orthotropic plate under a fractional-order derivative model is investigated, and efficient numerical simulations are achieved using the FKV fractional-order model and the shifted Legendre polynomial algorithm. The main conclusions include the following:

(1) The algorithm based on shifted Legendre polynomials successfully solves the governing equations under the fractional-order model with the error kept at a low level.
(2) An augmentation in the amplitude and frequency of dynamic loading results in heightened plate displacement, whilst an increase in plate thickness corresponds to a reduction in displacement.
(3) Fractional-order derivative models have superior accuracy in simulating the actual dynamics response of the plate relative to integer-order models.
(4) An augmentation in creep duration results in a reduction in displacement under particular fractional-order conditions.

Moreover, the future research directions are quite promising and we can further explore by applying other types of fractional differential equations to the dynamic response of viscoelastic materials. The dynamic response of complex structures in multiple physical

fields (e.g., thermal, electric, magnetic, etc.) can also be considered, and fractional-order derivatives can be introduced to model the interaction and coupling effects of these fields. With the wide application of smart materials (e.g., shape memory alloys, piezoelectric materials, etc.), exploring the dynamic response and performance prediction of fractional-order derivatives in these materials is also a compelling research direction.

Concurrently, we propose areas for enhancement, and in the future, we will conduct a more in-depth analysis of the specific mechanisms by which fractional-order derivatives influence the dynamic response of the plate, as well as a sensitivity analysis regarding the impact of various parameter fluctuations on the outcomes.

Author Contributions: Methodology, Y.C. (Yiming Chen); Writing—original draft, Q.F.; Writing—review & editing, Q.L. and L.W.; Visualization, Q.F.; Supervision, Y.C. (Yuhuan Cui) and J.Q. All authors have read and agreed to the published version of the manuscript.

Funding: This work is supported by National Natural Science Foundation of China (52074126), the Natural Science Foundation of Hebei Province (E2022209110) in China.

Data Availability Statement: No data were used for the research described in the article.

Conflicts of Interest: The authors declare no conflicts of interest.

Abbreviation

The following abbreviation is used in this manuscript:

FKV Fractional Kelvin–Voigt

References

1. Safarpour, M.; Ghabussi, A.; Ebrahimi, F.; Habibi, M.; Safarpour, H. Frequency characteristics of FG-GPLRC viscoelastic thick annular plate with the aid of GDQM. *Thin-Walled Struct.* **2020**, *150*, 106683. [CrossRef]
2. Zhao, J.; Zheng, L.; Zhang, X.; Liu, F. Unsteady natural convection boundary layer heat transfer of fractional Maxwell viscoelastic fluid over a vertical plate. *Int. J. Heat Mass Transf.* **2016**, *97*, 760–766. [CrossRef]
3. Zhu, S.; Cai, C.; Spanos, P.D. A nonlinear and fractional derivative viscoelastic model for rail pads in the dynamic analysis of coupled vehicle–slab track systems. *J. Sound Vib.* **2015**, *335*, 304–320. [CrossRef]
4. De, P.S.; De, R. Stick-slip dynamics of migrating cells on viscoelastic substrates. *Phys. Rev. E* **2019**, *100*, 012409. [CrossRef] [PubMed]
5. Zhang, Y.; Birgisson, B.; Lytton, R.L. Weak form equation–based finite-element modeling of viscoelastic asphalt mixtures. *J. Mater. Civ. Eng.* **2016**, *28*, 04015115. [CrossRef]
6. Zhang, X.; Li, Z.; Wang, X.; Yu, J. The fractional Kelvin-Voigt model for circumferential guided waves in a viscoelastic FGM hollow cylinder. *Appl. Math. Model.* **2021**, *89*, 299–313. [CrossRef]
7. Cao, J.; Chen, Y.; Wang, Y.; Zhang, H. Numerical analysis of nonlinear variable fractional viscoelastic arch based on shifted Legendre polynomials. *Math. Methods Appl. Sci.* **2021**, *44*, 8798–8813. [CrossRef]
8. Sun, L.; Chen, Y.; Dang, R.; Cheng, G.; Xie, J. Shifted Legendre polynomials algorithm used for the numerical analysis of viscoelastic plate with a fractional order model. *Math. Comput. Simul.* **2022**, *193*, 190–203. [CrossRef]
9. Brun, M.; Cortés, F.; Elejabarrieta, M.J. Transient Dynamic Analysis of Unconstrained Layer Damping Beams Characterized by a Fractional Derivative Model. *Mathematics* **2021**, *9*, 1731. [CrossRef]
10. Zvyagin, A.; Kostenko, E. Investigation of the weak solvability of one viscoelastic fractional Voigt model. *Mathematics* **2023**, *11*, 4472. [CrossRef]
11. Du, M.; Wang, Z.; Hu, H. Measuring memory with the order of fractional derivative. *Sci. Rep.* **2013**, *3*, 3431. [CrossRef]
12. Meng, R.; Yin, D.; Drapaca, C.S. Variable-order fractional description of compression deformation of amorphous glassy polymers. *Comput. Mech.* **2019**, *64*, 163–171. [CrossRef]
13. Mashayekhi, S.; Miles, P.; Hussaini, M.Y.; Oates, W.S. Fractional viscoelasticity in fractal and non-fractal media: Theory, experimental validation, and uncertainty analysis. *J. Mech. Phys. Solids* **2018**, *111*, 134–156. [CrossRef]
14. Ramirez, L.E.; Coimbra, C.F. A variable order constitutive relation for viscoelasticity. *Ann. Phys.* **2007**, *519*, 543–552. [CrossRef]
15. Sweilam, N.H.; Al-Mekhlafi, S.M. Numerical study for multi-strain tuberculosis (TB) model of variable-order fractional derivatives. *J. Adv. Res.* **2016**, *7*, 271–283. [CrossRef]

16. Lorenzo, C.F.; Hartley, T.T. Initialization, conceptualization, and application in the generalized (fractional) calculus. *Crit. Rev. Biomed. Eng.* **2007**, *35*, 447–553. [CrossRef]
17. Luchko, Y.; Gorenflo, R. An operational method for solving fractional differential equations with the Caputo derivatives. *Acta Math. Vietnam* **1999**, *24*, 207–233.
18. Diethelm, K.; Ford, N. *The Analysis of Fractional Differential Equations*; Lecture Notes in Mathematics; Springer: Berlin/Heidelberg, Germany, 2010; Volume 2004.
19. Fahad, H.M.; Fernandez, A. Operational calculus for Caputo fractional calculus with respect to functions and the associated fractional differential equations. *Appl. Math. Comput.* **2021**, *409*, 126400. [CrossRef]
20. Permoon, M.; Haddadpour, H.; Javadi, M. Nonlinear vibration of fractional viscoelastic plate: Primary, subharmonic, and superharmonic response. *Int. J. Non-Linear Mech.* **2018**, *99*, 154–164. [CrossRef]
21. Lei, Y.; Friswell, M.I.; Adhikari, S. A Galerkin method for distributed systems with non-local damping. *Int. J. Solids Struct.* **2006**, *43*, 3381–3400. [CrossRef]
22. Chazal, C.; Pitti, R.M. Integral approach for time dependent materials using finite element method. *J. Theor. Appl. Mech.* **2011**, *49*, 1029–1048.
23. Karakoç, S.B.G.; Uçar, Y.; Yağmurlu, N.M. Numerical solutions of the MRLW equation by cubic B-spline Galerkin finite element method. *Kuwait J. Sci. Eng.* **2015**, *42*, 141–159.
24. Neng-hui, Z.; Chang-jun, C. Non-linear mathematical model of viscoelastic thin plates with its applications. *Comput. Methods Appl. Mech. Eng.* **1998**, *165*, 307–319. [CrossRef]
25. Vivas-Cortez, M.; Yousif, M.A.; Mohammed, P.O.; Lupas, A.A.; Ibrahim, I.S.; Chorfi, N. Hyperbolic non-polynomial spline approach for time-fractional coupled KdV equations: A computational investigation. *Symmetry* **2024**, *16*, 1610. [CrossRef]
26. Cao, B.; Wu, X.; Wang, Y.; Zhu, Z. Modified hybrid B-spline estimation based on spatial regulator tensor network for burger equation with nonlinear fractional calculus. *Math. Comput. Simul.* **2024**, *220*, 253–275. [CrossRef]
27. Pezza, L.; Pitolli, F. A fractional spline collocation-Galerkin method for the time-fractional diffusion equation. *Commun. Appl. Ind. Math.* **2018**, *9*, 104–120. [CrossRef]
28. Yousif, M.A.; Hamasalh, F.K.; Zeeshan, A.; Abdelwahed, M. Efficient simulation of Time-Fractional Korteweg-de Vries equation via conformable-Caputo non-Polynomial spline method. *PLoS ONE* **2024**, *19*, e0303760. [CrossRef]
29. Vivas-Cortez, M.; Yousif, M.A.; Mahmood, B.A.; Mohammed, P.O.; Chorfi, N.; Lupas, A.A. High-Accuracy Solutions to the Time-Fractional KdV–Burgers Equation Using Rational Non-Polynomial Splines. *Symmetry* **2024**, *17*, 16. [CrossRef]
30. Wang, L.P.; Chen, Y.M.; Liu, D.Y.; Boutat, D. Numerical algorithm to solve generalized fractional pantograph equations with variable coefficients based on shifted Chebyshev polynomials. *Int. J. Comput. Math.* **2019**, *96*, 2487–2510. [CrossRef]
31. Chen, Y.M.; Wei, Y.Q.; Liu, D.Y.; Yu, H. Numerical solution for a class of nonlinear variable order fractional differential equations with Legendre wavelets. *Appl. Math. Lett.* **2015**, *46*, 83–88. [CrossRef]
32. Hassani, H.; Machado, J.T.; Naraghirad, E. An efficient numerical technique for variable order time fractional nonlinear Klein-Gordon equation. *Appl. Numer. Math.* **2020**, *154*, 260–272. [CrossRef]
33. Zheng, M.; Ma, H.; Lyu, Y.; Lu, C.; He, C. Derivation of circumferential guided waves equations for a multilayered laminate composite hollow cylinder by state-vector and Legendre polynomial hybrid formalism. *Compos. Struct.* **2021**, *255*, 112950. [CrossRef]
34. Pagani, A.d.; De Miguel, A.; Petrolo, M.; Carrera, E. Analysis of laminated beams via Unified Formulation and Legendre polynomial expansions. *Compos. Struct.* **2016**, *156*, 78–92. [CrossRef]
35. Srinivas, S.; Rao, A. Bending, vibration and buckling of simply supported thick orthotropic rectangular plates and laminates. *Int. J. Solids Struct.* **1970**, *6*, 1463–1481. [CrossRef]
36. Martinez, O.; Sankar, B.; Haftka, R.; Blosser, M.L. Two-dimensional orthotropic plate analysis for an integral thermal protection system. *AIAA J.* **2012**, *50*, 387–398. [CrossRef]
37. Zhou, K.; Su, J.; Hua, H. Aero-thermo-elastic flutter analysis of supersonic moderately thick orthotropic plates with general boundary conditions. *Int. J. Mech. Sci.* **2018**, *141*, 46–57. [CrossRef]
38. Vishnuvardhan, J.; Krishnamurthy, C.; Balasubramaniam, K. Genetic algorithm based reconstruction of the elastic moduli of orthotropic plates using an ultrasonic guided wave single-transmitter-multiple-receiver SHM array. *Smart Mater. Struct.* **2007**, *16*, 1639. [CrossRef]
39. Alam, M.; Mishra, S.K. Thermo-mechanical post-critical analysis of nonlocal orthotropic plates. *Appl. Math. Model.* **2020**, *79*, 106–125. [CrossRef]
40. Wen, Z.; Hou, C.; Zhao, M.; Wan, X. A peridynamic model for non-Fourier heat transfer in orthotropic plate with uninsulated cracks. *Appl. Math. Model.* **2023**, *115*, 706–723. [CrossRef]
41. Hobiny, A.; Abbas, I.A. A study on the thermoelastic interaction in two-dimension orthotropic materials under the fractional derivative model. *Alex. Eng. J.* **2023**, *64*, 615–625. [CrossRef]

42. Abouelregal, A.E. Three-phase-lag thermoelastic heat conduction model with higher-order time-fractional derivatives. *Indian J. Phys.* **2020**, *94*, 1949–1963. [CrossRef]
43. Chinnaboon, B.; Panyatong, M.; Chucheepsakul, S. Orthotropic plates resting on viscoelastic foundations with a fractional derivative Kelvin-Voigt model. *Compos. Struct.* **2023**, *322*, 117400. [CrossRef]
44. Gao, K.; Gao, W.; Wu, D.; Song, C. Nonlinear dynamic stability of the orthotropic functionally graded cylindrical shell surrounded by Winkler-Pasternak elastic foundation subjected to a linearly increasing load. *J. Sound Vib.* **2018**, *415*, 147–168. [CrossRef]
45. Chen, Y.; Sun, Y.; Liu, L. Numerical solution of fractional partial differential equations with variable coefficients using generalized fractional-order Legendre functions. *Appl. Math. Comput.* **2014**, *244*, 847–858. [CrossRef]
46. Shermergor, T. On the use of fractional differentiation operators for the description of elastic-after effect properties of materials. *J. Appl. Mech. Tech. Phys.* **1966**, *7*, 85–87. [CrossRef]
47. Reddy, J.N. *Theory and Analysis of Elastic Plates and Shells*; CRC Press: Boca Raton, FL, USA, 2006.
48. Rouzegar, J.; Vazirzadeh, M.; Heydari, M.H. A fractional viscoelastic model for vibrational analysis of thin plate excited by supports movement. *Mech. Res. Commun.* **2020**, *110*, 103618. [CrossRef]
49. Khan, R.A.; Khalil, H. A new method based on legendre polynomials for solution of system of fractional order partial differential equations. *Int. J. Comput. Math.* **2014**, *91*, 2554–2567. [CrossRef]
50. Nemati, S.; Ordokhani, Y. Legendre expansion methods for the numerical solution of nonlinear 2D Fredholm integral equations of the second kind. *J. Appl. Math. Inform.* **2013**, *31*, 609–621. [CrossRef]

Disclaimer/Publisher's Note: The statements, opinions and data contained in all publications are solely those of the individual author(s) and contributor(s) and not of MDPI and/or the editor(s). MDPI and/or the editor(s) disclaim responsibility for any injury to people or property resulting from any ideas, methods, instructions or products referred to in the content.